Neutron-induced fission cross section of ^{nat}Pb and ^{209}Bi from threshold to 1 GeV: An improved parametrization

D. Tarrío,[1,*] L. Tassan-Got,[2] L. Audouin,[2] B. Berthier,[2] I. Duran,[1] L. Ferrant,[2] S. Isaev,[2] C. Le Naour,[2] C. Paradela,[1] C. Stephan,[2] D. Trubert,[2] U. Abbondanno,[3] G. Aerts,[4] F. Álvarez-Velarde,[5] S. Andriamonje,[4] J. Andrzejewski,[6] P. Assimakopoulos,[7] G. Badurek,[8] P. Baumann,[9] F. Bečvář,[10] F. Belloni,[3] E. Berthoumieux,[4] F. Calviño,[11] M. Calviani,[12,13] D. Cano-Ott,[5] R. Capote,[14,15] C. Carrapiço,[4,16] A. Carrillo de Albornoz,[16] P. Cennini,[13] V. Chepel,[17] E. Chiaveri,[13] N. Colonna,[18] G. Cortes,[19] A. Couture,[20] J. Cox,[20] M. Dahlfors,[13] S. David,[2] I. Dillmann,[21] R. Dolfini,[22] C. Domingo-Pardo,[23] W. Dridi,[4] C. Eleftheriadis,[24] M. Embid-Segura,[5] A. Ferrari,[13] R. Ferreira-Marques,[17] L. Fitzpatrick,[13] H. Frais-Koelbl,[14] K. Fujii,[3] W. Furman,[25] I. Goncalves,[17] E. González-Romero,[5] A. Goverdovski,[26] F. Gramegna,[12] E. Griesmayer,[14] C. Guerrero,[5,13] F. Gunsing,[4] B. Haas,[27] R. Haight,[28] M. Heil,[29] A. Herrera-Martinez,[13] M. Igashira,[30] E. Jericha,[8] Y. Kadi,[13] F. Käppeler,[21] D. Karadimos,[7] D. Karamanis,[7] M. Kerveno,[9] V. Ketlerov,[25] P. Koehler,[31] V. Konovalov,[24] E. Kossionides,[32] M. Krtička,[10] C. Lampoudis,[4,24] H. Leeb,[8] C. Lederer,[33] A. Lindote,[17] I. Lopes,[17] R. Losito,[13] M. Lozano,[15] S. Lukic,[9] J. Marganiec,[6] L. Marques,[16] S. Marrone,[18] T. Martínez,[5] C. Massimi,[34] P. Mastinu,[12] E. Mendoza,[5] A. Mengoni,[14,13] P. M. Milazzo,[3] C. Moreau,[3] M. Mosconi,[21] F. Neves,[17] H. Oberhummer,[8] S. O'Brien,[20] M. Oshima,[35] J. Pancin,[4] C. Papachristodoulou,[7] C. Papadopoulos,[36] N. Patronis,[7] A. Pavlik,[37] P. Pavlopoulos,[38] L. Perrot,[4] M. T. Pigni,[8] R. Plag,[21] A. Plompen,[39] A. Plukis,[4] A. Poch,[19] J. Praena,[15] C. Pretel,[19] J. Quesada,[15] T. Rauscher,[40] R. Reifarth,[28] M. Rosetti,[41] C. Rubbia,[22] G. Rudolf,[9] P. Rullhusen,[39] J. Salgado,[16] C. Santos,[16] L. Sarchiapone,[13] R. Sarmento,[16] I. Savvidis,[24] G. Tagliente,[18] J. L. Tain,[23] L. Tavora,[16] R. Terlizzi,[18] G. Vannini,[34] P. Vaz,[16] A. Ventura,[41] D. Villamarin,[5] V. Vlachoudis,[13] R. Vlastou,[36] F. Voss,[21] S. Walter,[21] H. Wendler,[13] M. Wiescher,[20] and K. Wisshak[21]

(n_TOF Collaboration)

[1]*Universidade de Santiago de Compostela, Santiago de Compostela, Spain*
[2]*Centre National de la Recherche Scientifique/IN2P3, IPN, Orsay, France*
[3]*Istituto Nazionale di Fisica Nucleare, Trieste, Italy*
[4]*CEA/Saclay, IRFU, Gif-sur-Yvette, France*
[5]*Centro de Investigaciones Energeticas Medioambientales y Tecnologicas, Madrid, Spain*
[6]*University of Lodz, Lodz, Poland*
[7]*University of Ioannina, Ioannina, Greece*
[8]*Atominstitut der Österreichischen Universitäten, Technische Universität Wien, Vienna, Austria*
[9]*Centre National de la Recherche Scientifique/IN2P3, IReS, Strasbourg, France*
[10]*Charles University, Prague, Czech Republic*
[11]*Universidad Politecnica de Catalunya, Barcelona, Spain*
[12]*Laboratori Nazionali di Legnaro, Istituto Nazionale di Fisica Nucleare, Legnaro, Italy*
[13]*CERN, Geneva, Switzerland*
[14]*Nuclear Data Section, International Atomic Energy Agency (IAEA), Vienna, Austria*
[15]*Universidad de Sevilla, Seville, Spain*
[16]*Instituto Tecnológico e Nuclear (ITN), Lisbon, Portugal*
[17]*LIP-Coimbra and Departamento de Fisica da Universidade de Coimbra, Coimbra, Portugal*
[18]*Istituto Nazionale di Fisica Nucleare, Bari, Italy*
[19]*Universitat Politecnica de Catalunya, Barcelona, Spain*
[20]*University of Notre Dame, Notre Dame, Indiana 46556, USA*
[21]*Karlsruhe Institute of Technology (KIT), Institut für Kernphysik, Karlsruhe, Germany*
[22]*Università degli Studi Pavia, Pavia, Italy*
[23]*Instituto de Física Corpuscular, CSIC-Universidad de Valencia, Valencia, Spain*
[24]*Aristotle University of Thessaloniki, Thessaloniki, Greece*
[25]*Joint Institute for Nuclear Research, Frank Laboratory of Neutron Physics, Dubna, Russia*
[26]*Institute of Physics and Power Engineering, Kaluga Region, Obninsk, Russia*
[27]*Centre National de la Recherche Scientifique/IN2P3, CENBG, Bordeaux, France*
[28]*Los Alamos National Laboratory, Los Alamos, New Mexico 87545, USA*
[29]*GSI, Darmstadt, Germany*
[30]*Tokyo Institute of Technology, Tokyo, Japan*
[31]*Physics Division, Oak Ridge National Laboratory, Oak Ridge, Tennessee 37831, USA*
[32]*NCSR, Athens, Greece*
[33]*Faculty of Physics, University of Vienna, Vienna, Austria*
[34]*Dipartimento di Fisica, Università di Bologna, and Sezione INFN di Bologna, Bologna, Italy*
[35]*Japan Atomic Energy Research Institute, Tokai-mura, Ibaraki, Japan*
[36]*National Technical University of Athens, Athens, Greece*
[37]*Institut für Isotopenforschung und Kernphysik, Universität Wien, Vienna, Austria*

[38] *Pôle Universitaire Léonard de Vinci, Paris La Défense, France*
[39] *CEC-JRC-IRMM, Geel, Belgium*
[40] *Department of Physics, University of Basel, Basel, Switzerland*
[41] *ENEA, Bologna, Italy*
(Received 10 February 2011; published 28 April 2011)

Neutron-induced fission cross sections for ^{nat}Pb and ^{209}Bi were measured with a white-spectrum neutron source at the CERN Neutron Time-of-Flight (n_TOF) facility. The experiment, using neutrons from threshold up to 1 GeV, provides the first results for these nuclei above 200 MeV. The cross sections were measured relative to ^{235}U and ^{238}U in a dedicated fission chamber with parallel plate avalanche counter detectors. Results are compared with previous experimental data. Upgraded parametrizations of the cross sections are presented, from threshold energy up to 1 GeV. The proposed new sets of fitting parameters improve former results along the whole energy range.

DOI: 10.1103/PhysRevC.83.044620 PACS number(s): 25.85.Ec, 28.65.+a, 29.25.Dz, 28.41.−i

I. INTRODUCTION

Data on neutron-induced fission cross sections at intermediate energies are crucial for the development of accelerator-driven systems. ^{nat}Pb and ^{209}Bi play a key role, because liquid lead-bismuth eutectic is the reference spallation target material [1]. The fission induced by high-energy neutrons in these structural materials determines the neutron spectrum shape, the extent of the target heating, and the remaining radioactivity of the target.

These data are also important in fundamental nuclear physics. The fission of subactinide nuclei, for example, is instrumental in studying the effect of the transient time, where saddle configurations are more elongated.

^{209}Bi(n,f) was recommended as a cross section reference nucleus for neutron energies above 50 MeV, but new measurements are requested [2]. Because of its high threshold (about 20 MeV), it can be used as a fluence monitor for high-energy neutrons, even when a low-energy neutron background is present. In addition, ^{209}Bi is a monoisotopic, nonradioactive material that shows a smooth dependence of the fission cross section on neutron energy, making it very well suited for this purpose.

The present work provides a new set of high-precision measurements for the ^{209}Bi(n,f) and ^{nat}Pb(n,f) cross sections, covering the entire energy range from threshold up to 1 GeV. The high-intensity neutron beam of the CERN Neutron Time-of-Flight (n_TOF) facility compensates for the low cross section values. The results presented here are part of an experimental campaign on fission cross sections performed with the same detection setup [3,4].

II. EXPERIMENTAL METHOD

The experiment was performed at the CERN n_TOF facility [5]. A very intense neutron flux was produced by spallation reactions on a lead target using a 20 GeV/c proton beam from the Proton Synchrotron at CERN. The cooling water surrounding the spallation target acted as a moderator to produce a neutron flux covering a wide energy range. The long, 185-m flight path between the spallation target and the experimental area makes it possible to obtain high-resolution time-of-flight (TOF) measurements. Presently, n_TOF is the only neutron facility that can cover the whole energy range from thermal energy to 1 GeV. More detailed descriptions can be found in the literature [6,7].

The fission fragments were detected in a reaction chamber with parallel plate avalanche counters (PPACs) that were developed at IPN Orsay [8–10], using ^{235}U and ^{238}U as reference samples for defining the neutron flux.

A. Parallel plate avalanche counter

The PPACs used in this experiment have a central anode flanked by two cathodes. A low-pressure gas fills the 3-mm gaps between the 1.5-μm aluminized Mylar foil electrodes. The cathodes of each PPAC were segmented in perpendicular directions so that the fission fragment trajectory could be reconstructed. PPAC anode signals are very fast (9 ns width at half maximum), which reduces the pileup probabilities and makes it possible to reach energies as high as 1 GeV.

The reaction chamber contained 10 PPACs, with 9 targets in between them, all placed perpendicular to the direction of the neutron beam. The fission events were identified as coincidence signals in the anodes of two consecutive PPACs. A very detailed description of the chamber and the PPACs can be found in Ref. [10].

B. Targets

The samples used in this work were produced by different methods. The ^{nat}Pb and ^{209}Bi samples were the result of vacuum evaporation deposition on a 240-μg/cm^2 extended Mylar foil, while the ^{235}U and ^{238}U samples were produced by electrodeposition on a 2.5-μm-thick aluminum foil. Both U samples were 8 cm in diameter. The mass distributions, the total masses, and the chemical compositions of the samples and backings were determined by Rutherford backscattering spectroscopy. The ^{235}U and ^{238}U masses were also measured independently by α spectroscopy. Isotopic impurities of ^{238}U (6.28% in number of atoms), ^{234}U (0.74%), and ^{236}U (0.27%) were found in the ^{235}U sample [10]. The counting rate for this target was corrected to account for the fission cross sections of these contaminants.

*diego.tarrio@usc.es

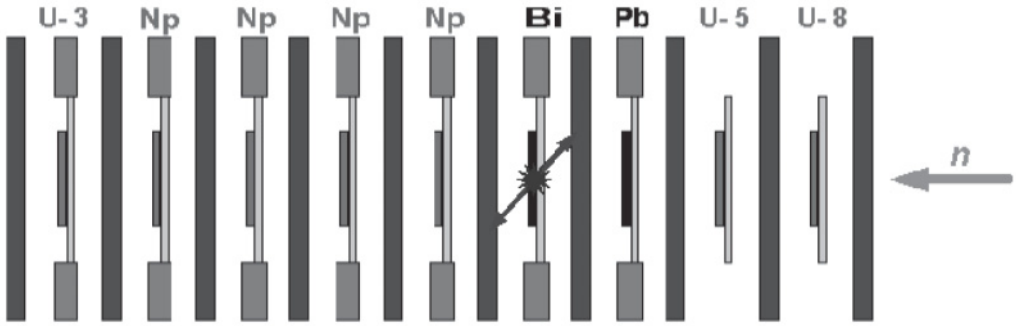

FIG. 1. Schematic view of the PPAC detectors and the samples used in this experiment.

Figure 1 shows the 10 PPACs and the 9 samples used in the experiment: one ^{233}U target, four ^{237}Np targets, one ^{209}Bi target, one ^{nat}Pb target, and the ^{235}U and ^{238}U samples that were used as reference targets to measure the neutron flux. The fission cross sections of ^{237}Np and ^{233}U are reported in other works [3,4]. Because the PPACs and targets are relatively thin, the neutron beam intensity was reduced in the entire setup by less than 1%, as was indicated by a simulation using the MCNP code [11].

III. DATA ANALYSIS

Both fission fragments were emitted in opposite directions and were recorded in the adjacent PPACs within a coincidence window of 10 ns. This coincidence method rejects most of the background produced by α emission of the radioactive targets and by spallation reactions in the materials surrounding the samples. Additionally, the correlation between the time difference and the signal amplitude of the two PPAC anodes improves the identification of the fission events by removing random coincidences.

The neutron energy was measured by the TOF technique using γ flash signals for calibration. The γ flash consists of γ rays and ultrarelativistic light-charged particles produced when the proton beam hits the spallation target. It provides a common time reference within 1 ns for all the detectors. The maximum achievable energy in our experiment was limited by the width of the γ flash and corresponds to 1 GeV.

A. Cross section determination

The number of detected fission events (per unit of incident energy) induced by neutrons in a target during the full measuring time is

$$C(E) = \Phi(E)\, N\, \sigma(E)\, \epsilon(E), \tag{1}$$

where $\Phi(E)$ is the time-integrated neutron fluence (measured in n cm^{-2} MeV^{-1}) for the full measuring time, N is the total number of atoms in the target, $\sigma(E)$ is the fission cross section of the isotope, and $\epsilon(E)$ is the detection efficiency. An additional correction for the counting rate from sample impurities must be included for ^{235}U. The ratio of fission cross sections for two of the samples is

$$\frac{\sigma_i(E)}{\sigma_j(E)} = \frac{C_i(E)}{C_j(E)} \frac{\Phi_j(E)}{\Phi_i(E)} \frac{N_j \epsilon_j(E)}{N_i \epsilon_i(E)}. \tag{2}$$

The mass densities of the targets were accurately measured as explained in Sec. II B. Differences in the neutron flux and the efficiency detection for different samples are explained in the following sections.

B. Beam spot correction

The samples differed in size and thus received different numbers of neutrons. The ^{235}U and ^{238}U samples were well-defined layers 8 cm in diameter and smaller than the beam size. The ^{nat}Pb and ^{209}Bi samples were spread over the entire Mylar layer, which was larger than the beam size. This is shown in Fig. 2, where the solid circle indicates the position of the ^{235}U reference sample. Using Eq. (1), the ratio of the number of fission events inside this circle with respect to the total number of fissions is given as

$$F = \frac{C_{\rm in}(E)}{C_{\rm tot}(E)} = \frac{\phi_{\rm in}(E)}{\phi_{\rm tot}(E)} \frac{S_{\rm in}}{S_{\rm tot}} \frac{n}{n} \frac{\sigma_f(E)}{\sigma_f(E)} \frac{\epsilon(E)}{\epsilon(E)}, \tag{3}$$

where $\phi_{\rm in}(E)$ and $\phi_{\rm tot}(E)$ are the density of neutrons (n cm^{-2}) that hit the target inside the circle and in the whole beam spot, n is the number of atoms per unit area in the sample, and $S_{\rm in}$ and $S_{\rm tot}$ are the areas of the circle and of the target region exposed to the beam. Cancellation of equal terms in this equation leads

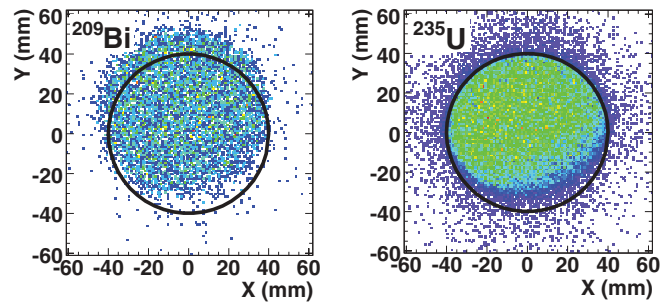

FIG. 2. (Color online) Position of fission events in ^{209}Bi and ^{235}U samples. The 8-cm circle shows the position of the ^{235}U reference sample.

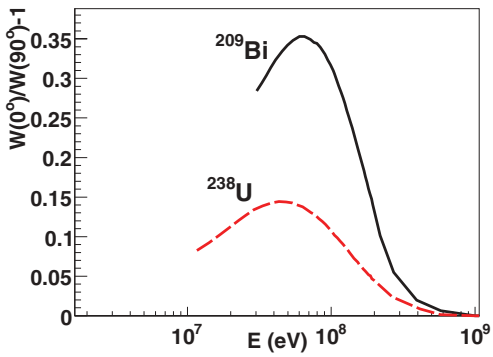

FIG. 3. (Color online) Parametrization of the anisotropy for ^{209}Bi and ^{238}U reported in Ref. [14] and extended up to 1 GeV assuming a decrease at the highest energies.

to a global correction factor for the different target sizes:

$$F = \frac{C_{\text{in}}(E)}{C_{\text{tot}}(E)} = \frac{\phi_{\text{in}}(E)}{\phi_{\text{tot}}(E)} \frac{S_{\text{in}}}{S_{\text{tot}}}. \quad (4)$$

By integrating the fission events inside the circle defined by the ^{235}U sample and the events in the whole target, a value of $F = 0.81 \pm 0.02$ was obtained to correct for the different sizes of the $^{\text{nat}}$Pb and ^{209}Bi samples with respect to the ^{235}U and ^{238}U samples.

C. Detection efficiency correction

The detection efficiency is an important issue for the cross section measurements. Although we impose the coincidence detection of both fission fragments, the angular acceptance is reduced because the fragments must pass through material layers before reaching the active part of the detector. The angular acceptance is different for the Pb/Bi and the U samples because of their different backings. For each sample, the maximum acceptance angle was determined by a Monte Carlo simulation and by calculating the fragment energy losses in the samples and backings based on the stopping power values of the respective materials. The thickness and the composition of the samples, backings, and material layers of the PPAC detectors were included. The mass distribution of the fission fragments for $^{\text{nat}}$Pb and ^{209}Bi is supposedly the same and was taken from a Gaussian fit to the experimental results of Ref. [12] for 30-MeV proton-induced fission of ^{209}Bi.

A random generator was used to select the initial fission fragment pair. A unique value of Z was assigned to each A value, keeping the ratio Z/A constant. The total kinetic energy, calculated using Viola's systematics [13], was distributed between both fission fragments following the inverse mass relation. For symmetric fission above 30 MeV, a Gaussian mass distribution was also assumed for the ^{235}U and ^{238}U samples. The dependence on the minimum energy thresholds imposed on the particles reaching the active region of the detectors was studied and average maximum acceptance angle values of 60° and 66° were found for the U and Pb/Bi samples, respectively.

The limited acceptance angle made it necessary to apply a suitable correction to account for the missing solid angle. The correction depends on the fission angular distributions. Because the PPACs are position sensitive, the distributions could be determined from the trajectory reconstruction. However, we did not use this because of the limited angular range covered by our system. Instead, we used the parametrization given in Ref. [14] for the anisotropy in neutron- and proton-induced fission of ^{209}Bi and ^{238}U. We extended the data above 200 MeV up to 1 GeV by means of a simple function (see Fig. 3) assuming that the anisotropy decreases in a manner analogous to ^{232}Th and ^{238}U [15].

Assuming that the angular distribution $W(\theta)$ of $^{\text{nat}}$Pb is very similar to that of ^{209}Bi, the correction factor for the detection efficiency is

$$f_\theta = \frac{\int_x^1 W(\theta)\, d(\cos\theta)}{\int_0^1 W(\theta)\, d(\cos\theta)}, \quad (5)$$

where x is the cosine of the maximum acceptance angle in each case. For example, the correction due to the angular distribution effect reaches a maximum of 10% at 30 MeV in the cross section ratio of ^{209}Bi and ^{238}U.

TABLE I. Systematic uncertainties in the fission cross sections presented in this work.

Contribution	Uncertainty (%)	
	$E < 100$ MeV	$E \geqslant 100$ MeV
Sample mass	1.2	1.2
Thickness and threshold effects	3.5	3.5
Beam spot size	2.5	2.5
Anisotropy	1	2
Total	4.6	4.9

IV. SYSTEMATIC UNCERTAINTIES

The total systematic uncertainty in the cross section is determined by the uncertainties associated with the different terms in Eq. (2). The mass of the targets, measured according to the explanation given in Sec. II B, introduces a systematic uncertainty of 1.2% [10].

The detection efficiency ratio contributes the largest systematic uncertainty due to differences in material thickness and detector thresholds. This uncertainty was previously estimated for this experiment by analyzing samples of the same isotope, where systematic effects could be separated [3].

The uncertainty in the anisotropy correction is less than 1% in the energy region below 100 MeV, where the anisotropy is largest. At higher energies, the anisotropy is not well known, so a 2% uncertainty was adopted. The different sample sizes add another systematic uncertainty of 2.5%, as was explained in Sec. III B. The total systematic uncertainty is shown in Table I as the quadratic sum of the different contributions.

V. EXPERIMENTAL RESULTS

In this work, we determined the cross section ratios for neutron-induced fission of $^{\text{nat}}$Pb and ^{209}Bi. For the first time,

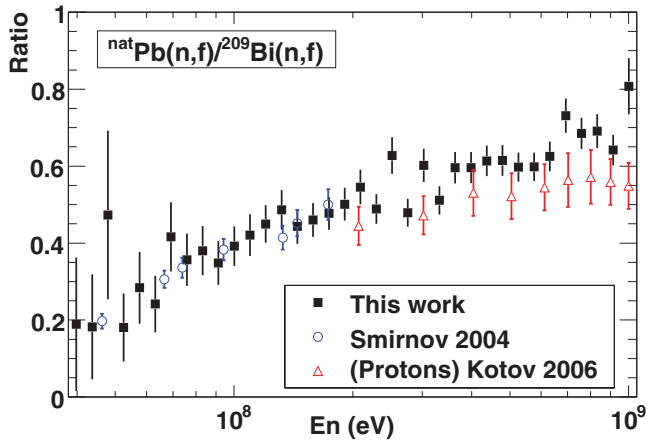

FIG. 4. (Color online) Fission cross section ratio of $\sigma_f(^{nat}\mathrm{Pb})/\sigma_f(^{209}\mathrm{Bi})$. Recent data obtained using neutrons [17] and high-energy protons [18] are also shown.

the energy range under investigation could be extended to 1 GeV. It should be stressed, also, that our results do not rely on any normalization to previous results or evaluations, because all the numerical factors were calculated as explained. Comparisons of our results with available data in the Experimental Nuclear Reaction Data (EXFOR) database [16] are shown for all cases.

A. Cross section ratios

The measured $\sigma_f(^{nat}\mathrm{Pb})/\sigma_f(^{209}\mathrm{Bi})$ ratio is plotted in Fig. 4. Comparison with recent results of Smirnov *et al.* [17] exhibits good agreement in the energy range below 200 MeV. Above this energy there are only data from proton-induced fission [18], which are systematically lower.

This ratio can be given with a fairly small uncertainty because no correction due to the different beam spot has to be applied, and the ratio of detection efficiency is assumed to be equal to unity. This ratio is especially interesting because

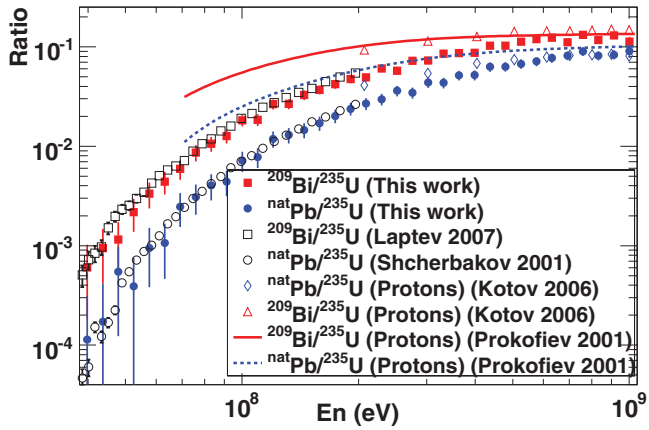

FIG. 5. (Color online) Fission cross section ratios for $^{nat}\mathrm{Pb}/^{235}\mathrm{U}$ and $^{209}\mathrm{Bi}/^{235}\mathrm{U}$ vs neutron incident energy. Our results are compared with previous references using neutrons [19,20] and protons [18]. Systematics from Ref. [21] for proton-induced fission are also shown.

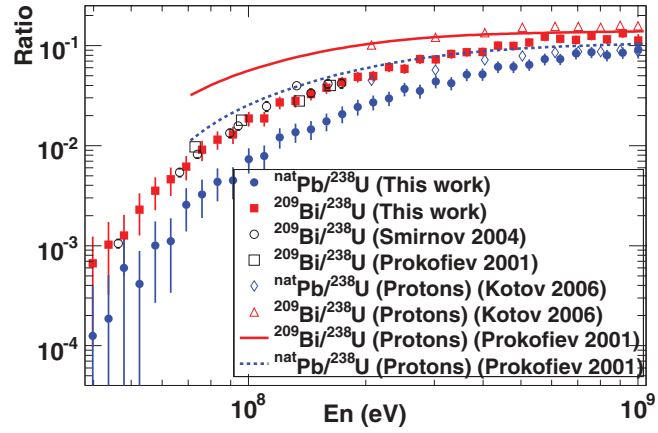

FIG. 6. (Color online) Fission cross section ratios for $^{nat}\mathrm{Pb}/^{238}\mathrm{U}$ and $^{209}\mathrm{Bi}/^{238}\mathrm{U}$ vs neutron incident energy. Our results are compared with previous references using neutrons [17,23] and protons [18]. Systematics from Ref. [21] are also shown.

^{209}Bi is likely to become a new reference for neutron-induced fission in the region of subactinides [2], so cross section ratios for fission in subactinides would be measured relative to it.

Ratios of ^{nat}Pb and ^{209}Bi with respect to ^{235}U are shown in Fig. 5. Data published by Laptev *et al.* [19] for the $^{209}\mathrm{Bi}/^{235}\mathrm{U}$ ratio and by Shcherbakov *et al.* [20] for $^{nat}\mathrm{Pb}/^{235}\mathrm{U}$ are also shown. In the region above 200 MeV, the proton-induced cross sections by Kotov *et al.* [18] and the systematics for proton-induced fission [21] are indicated for comparison. The present $^{209}\mathrm{Bi}/^{235}\mathrm{U}$ ratio is clearly lower than the data of Ref. [19], but the ^{nat}Pb results are in good agreement with the data set of Ref. [20]. In both cases, the proton-induced cross sections exhibit an energy dependence that is very different from the present results (except at very high energies). Although the statistical accuracy is limited at high energies because of the lower flux, our results indicate a trend to saturation around 600 and 700 MeV for ^{209}Bi and ^{nat}Pb, respectively.

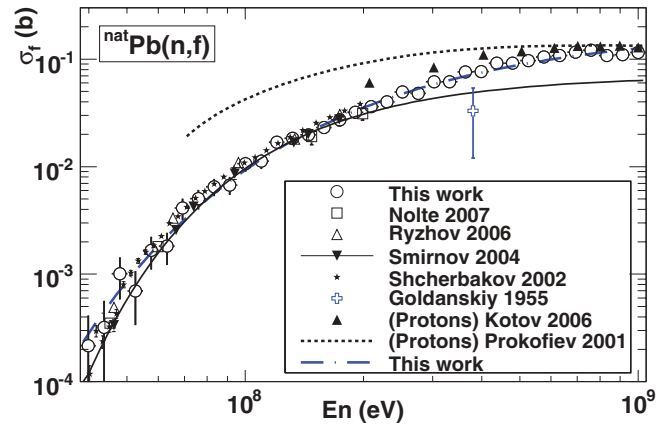

FIG. 7. (Color online) Neutron-induced fission cross section for ^{nat}Pb obtained at the n_TOF facility. Previous results using neutrons [17,20,26–28] are shown. The parametrization of Ref. [17] is compared with the new parametrization proposed in this work (see Sec. VI). Experimental results [18] and a systematics [21] for high-energy protons are also indicated.

TABLE II. Cross section ratios for neutron-induced fission and statistical uncertainties.

Energy (eV)	^{nat}Pb/^{209}Bi	^{nat}Pb/^{235}U	^{nat}Pb/^{238}U	^{209}Bi/^{235}U	^{209}Bi/^{238}U
4.37×10^7	0.18 ± 0.14	$(1.73 \pm 2.0) \times 10^{-4}$	$(1.86 \pm 3.0) \times 10^{-4}$	$(9.46 \pm 5.0) \times 10^{-4}$	$(1.02 \pm 0.7) \times 10^{-3}$
4.79×10^7	0.47 ± 0.22	$(5.47 \pm 4.0) \times 10^{-4}$	$(5.99 \pm 6.0) \times 10^{-4}$	$(1.16 \pm 0.6) \times 10^{-3}$	$(1.27 \pm 0.8) \times 10^{-3}$
5.25×10^7	0.18 ± 0.09	$(3.91 \pm 4.0) \times 10^{-4}$	$(4.15 \pm 5.0) \times 10^{-4}$	$(2.17 \pm 0.8) \times 10^{-3}$	$(2.30 \pm 1.0) \times 10^{-3}$
5.76×10^7	0.28 ± 0.09	$(9.49 \pm 6.0) \times 10^{-4}$	$(1.01 \pm 0.7) \times 10^{-3}$	$(3.34 \pm 1.0) \times 10^{-3}$	$(3.55 \pm 1.0) \times 10^{-3}$
6.32×10^7	0.24 ± 0.07	$(1.07 \pm 0.6) \times 10^{-3}$	$(1.11 \pm 0.8) \times 10^{-3}$	$(4.41 \pm 1.0) \times 10^{-3}$	$(4.60 \pm 1.0) \times 10^{-3}$
6.93×10^7	0.42 ± 0.09	$(2.46 \pm 0.9) \times 10^{-3}$	$(2.57 \pm 1.0) \times 10^{-3}$	$(5.91 \pm 1.0) \times 10^{-3}$	$(6.17 \pm 2.0) \times 10^{-3}$
7.59×10^7	0.36 ± 0.07	$(3.08 \pm 1.0) \times 10^{-3}$	$(3.24 \pm 1.0) \times 10^{-3}$	$(8.65 \pm 2.0) \times 10^{-3}$	$(9.09 \pm 2.0) \times 10^{-3}$
8.33×10^7	0.38 ± 0.06	$(4.03 \pm 1.0) \times 10^{-3}$	$(4.36 \pm 2.0) \times 10^{-3}$	$(1.06 \pm 0.2) \times 10^{-2}$	$(1.15 \pm 0.2) \times 10^{-2}$
9.13×10^7	0.35 ± 0.06	$(4.41 \pm 1.0) \times 10^{-3}$	$(4.50 \pm 2.0) \times 10^{-3}$	$(1.27 \pm 0.2) \times 10^{-2}$	$(1.29 \pm 0.3) \times 10^{-2}$
1.00×10^8	0.39 ± 0.05	$(7.16 \pm 2.0) \times 10^{-3}$	$(7.32 \pm 2.0) \times 10^{-3}$	$(1.83 \pm 0.2) \times 10^{-2}$	$(1.87 \pm 0.3) \times 10^{-2}$
1.10×10^8	0.42 ± 0.05	$(7.78 \pm 2.0) \times 10^{-3}$	$(7.86 \pm 2.0) \times 10^{-3}$	$(1.85 \pm 0.3) \times 10^{-2}$	$(1.87 \pm 0.3) \times 10^{-2}$
1.20×10^8	0.45 ± 0.05	$(1.19 \pm 0.2) \times 10^{-2}$	$(1.21 \pm 0.3) \times 10^{-2}$	$(2.64 \pm 0.3) \times 10^{-2}$	$(2.70 \pm 0.4) \times 10^{-2}$
1.32×10^8	0.49 ± 0.05	$(1.30 \pm 0.2) \times 10^{-2}$	$(1.36 \pm 0.3) \times 10^{-2}$	$(2.66 \pm 0.3) \times 10^{-2}$	$(2.80 \pm 0.4) \times 10^{-2}$
1.45×10^8	0.44 ± 0.04	$(1.45 \pm 0.3) \times 10^{-2}$	$(1.45 \pm 0.3) \times 10^{-2}$	$(3.27 \pm 0.4) \times 10^{-2}$	$(3.28 \pm 0.4) \times 10^{-2}$
1.59×10^8	0.46 ± 0.04	$(1.70 \pm 0.3) \times 10^{-2}$	$(1.74 \pm 0.4) \times 10^{-2}$	$(3.70 \pm 0.4) \times 10^{-2}$	$(3.79 \pm 0.5) \times 10^{-2}$
1.74×10^8	0.48 ± 0.04	$(2.01 \pm 0.3) \times 10^{-2}$	$(2.07 \pm 0.4) \times 10^{-2}$	$(4.22 \pm 0.4) \times 10^{-2}$	$(4.33 \pm 0.5) \times 10^{-2}$
1.91×10^8	0.50 ± 0.04	$(2.37 \pm 0.3) \times 10^{-2}$	$(2.43 \pm 0.4) \times 10^{-2}$	$(4.73 \pm 0.5) \times 10^{-2}$	$(4.86 \pm 0.6) \times 10^{-2}$
2.09×10^8	0.55 ± 0.05	$(2.68 \pm 0.4) \times 10^{-2}$	$(2.71 \pm 0.5) \times 10^{-2}$	$(4.92 \pm 0.5) \times 10^{-2}$	$(4.97 \pm 0.6) \times 10^{-2}$
2.29×10^8	0.49 ± 0.04	$(2.97 \pm 0.4) \times 10^{-2}$	$(2.97 \pm 0.5) \times 10^{-2}$	$(6.07 \pm 0.5) \times 10^{-2}$	$(6.07 \pm 0.7) \times 10^{-2}$
2.51×10^8	0.63 ± 0.05	$(3.61 \pm 0.4) \times 10^{-2}$	$(3.68 \pm 0.6) \times 10^{-2}$	$(5.75 \pm 0.5) \times 10^{-2}$	$(5.86 \pm 0.7) \times 10^{-2}$
2.76×10^8	0.48 ± 0.04	$(3.45 \pm 0.4) \times 10^{-2}$	$(3.51 \pm 0.6) \times 10^{-2}$	$(7.21 \pm 0.6) \times 10^{-2}$	$(7.33 \pm 0.8) \times 10^{-2}$
3.02×10^8	0.60 ± 0.04	$(4.38 \pm 0.5) \times 10^{-2}$	$(4.38 \pm 0.6) \times 10^{-2}$	$(7.27 \pm 0.6) \times 10^{-2}$	$(7.28 \pm 0.8) \times 10^{-2}$
3.31×10^8	0.51 ± 0.04	$(4.34 \pm 0.5) \times 10^{-2}$	$(4.21 \pm 0.6) \times 10^{-2}$	$(8.50 \pm 0.7) \times 10^{-2}$	$(8.23 \pm 0.8) \times 10^{-2}$
3.63×10^8	0.60 ± 0.04	$(5.16 \pm 0.6) \times 10^{-2}$	$(5.12 \pm 0.7) \times 10^{-2}$	$(8.66 \pm 0.7) \times 10^{-2}$	$(8.59 \pm 0.9) \times 10^{-2}$
3.99×10^8	0.60 ± 0.04	$(5.19 \pm 0.6) \times 10^{-2}$	$(5.16 \pm 0.7) \times 10^{-2}$	$(8.70 \pm 0.7) \times 10^{-2}$	$(8.65 \pm 0.9) \times 10^{-2}$
4.37×10^8	0.61 ± 0.04	$(6.28 \pm 0.7) \times 10^{-2}$	$(6.14 \pm 0.8) \times 10^{-2}$	$(1.02 \pm 0.08) \times 10^{-1}$	$(1.00 \pm 0.1) \times 10^{-1}$
4.79×10^8	0.61 ± 0.04	$(6.30 \pm 0.7) \times 10^{-2}$	$(6.12 \pm 0.8) \times 10^{-2}$	$(1.02 \pm 0.08) \times 10^{-1}$	$(9.95 \pm 1.0) \times 10^{-2}$
5.25×10^8	0.60 ± 0.04	$(6.74 \pm 0.7) \times 10^{-2}$	$(6.43 \pm 0.9) \times 10^{-2}$	$(1.13 \pm 0.09) \times 10^{-1}$	$(1.08 \pm 0.1) \times 10^{-1}$
5.76×10^8	0.60 ± 0.04	$(7.13 \pm 0.8) \times 10^{-2}$	$(7.32 \pm 1.0) \times 10^{-2}$	$(1.19 \pm 0.09) \times 10^{-1}$	$(1.22 \pm 0.1) \times 10^{-1}$
6.32×10^8	0.63 ± 0.04	$(7.71 \pm 0.8) \times 10^{-2}$	$(7.30 \pm 0.9) \times 10^{-2}$	$(1.23 \pm 0.1) \times 10^{-1}$	$(1.17 \pm 0.1) \times 10^{-1}$
6.93×10^8	0.73 ± 0.04	$(8.14 \pm 0.8) \times 10^{-2}$	$(8.34 \pm 1.0) \times 10^{-2}$	$(1.11 \pm 0.09) \times 10^{-1}$	$(1.14 \pm 0.1) \times 10^{-1}$
7.59×10^8	0.68 ± 0.04	$(9.01 \pm 0.9) \times 10^{-2}$	$(8.57 \pm 1.0) \times 10^{-2}$	$(1.32 \pm 0.1) \times 10^{-1}$	$(1.25 \pm 0.1) \times 10^{-1}$
8.33×10^8	0.69 ± 0.04	$(8.11 \pm 0.9) \times 10^{-2}$	$(8.00 \pm 1.0) \times 10^{-2}$	$(1.17 \pm 0.1) \times 10^{-1}$	$(1.16 \pm 0.1) \times 10^{-1}$
9.13×10^8	0.64 ± 0.04	$(8.33 \pm 0.9) \times 10^{-2}$	$(8.49 \pm 1.0) \times 10^{-2}$	$(1.30 \pm 0.1) \times 10^{-1}$	$(1.32 \pm 0.1) \times 10^{-1}$
1.00×10^9	0.81 ± 0.07	$(9.07 \pm 1.0) \times 10^{-2}$	$(9.10 \pm 2.0) \times 10^{-2}$	$(1.12 \pm 0.1) \times 10^{-1}$	$(1.13 \pm 0.2) \times 10^{-1}$

The ratios of ^{nat}Pb and ^{209}Bi with respect to ^{238}U are shown in Fig. 6. We compared our results with earlier data of Smirnov *et al.* [17] (based on the previous work of Eismont *et al.* [22]) as well as with the experimental data from Prokofiev [23]. These data agree well with ours within their measured energy ranges (up to 200 MeV). Dashed lines represent the systematics of Prokofiev [21] for proton-induced fission. Concerning the proton data, both for the Prokofiev systematics and for the Kotov *et al.* measurements, the same trend as for the ratios over ^{235}U is observed.

Numerical results for the fission cross section ratios are shown in Table II along with the statistical uncertainty. A logarithmic energy binning of 25 bins/decade was used.

The (n, f) standard cross sections of ^{235}U and ^{238}U [24] are limited to energies below 200 MeV. Therefore, we used the Japanese Evaluated Nuclear Data Library High Energy File (JENDL/HE-2007) [25] to obtain the cross sections of ^{nat}Pb(n, f) and ^{209}Bi(n, f), because it covers our whole energy range. The experimental values of the cross sections for both ^{nat}Pb and ^{209}Bi are listed in Table III.

B. The ^{nat}Pb(n, f) cross section

The final result for the neutron-induced fission cross section of ^{nat}Pb, extended up to 1 GeV for the first time, is shown in Fig. 7. Published data by Nolte *et al.* [26], Ryzhov *et al.* [27], Smirnov *et al.* [17], and Shcherbakov *et al.* [20] with neutrons below 200 MeV are available in the EXFOR database [16] and are in agreement with this work within the statistical uncertainties. However, this is not the case with the earlier measurement of Goldanskiy *et al.* at 380 MeV [28], which underestimates the cross section. Above 200 MeV, essentially only proton data [18] and the systematics of Prokofiev [21] are available for comparison. The latter is in agreement with our data only at the highest energies, where the (p, f) and (n, f) cross sections are expected to converge.

TABLE III. Neutron-induced fission cross sections of ^{nat}Pb and ^{209}Bi with their statistical uncertainties.

Energy (eV)	$\sigma_f(^{nat}\text{Pb})$ (b)	$\sigma_f(^{209}\text{Bi})$ (b)
4.37×10^7	$(3.19 \pm 2.0) \times 10^{-4}$	$(1.75 \pm 0.5) \times 10^{-3}$
4.79×10^7	$(1.01 \pm 0.4) \times 10^{-3}$	$(2.13 \pm 0.6) \times 10^{-3}$
5.25×10^7	$(6.99 \pm 4.0) \times 10^{-4}$	$(3.87 \pm 0.8) \times 10^{-3}$
5.76×10^7	$(1.67 \pm 0.6) \times 10^{-3}$	$(5.87 \pm 1.0) \times 10^{-3}$
6.32×10^7	$(1.82 \pm 0.6) \times 10^{-3}$	$(7.54 \pm 1.0) \times 10^{-3}$
6.93×10^7	$(4.11 \pm 0.9) \times 10^{-3}$	$(9.88 \pm 1.0) \times 10^{-3}$
7.59×10^7	$(5.05 \pm 1.0) \times 10^{-3}$	$(1.42 \pm 0.2) \times 10^{-2}$
8.33×10^7	$(6.51 \pm 1.0) \times 10^{-3}$	$(1.71 \pm 0.2) \times 10^{-2}$
9.13×10^7	$(6.73 \pm 1.0) \times 10^{-3}$	$(1.93 \pm 0.2) \times 10^{-2}$
1.00×10^8	$(1.07 \pm 0.2) \times 10^{-2}$	$(2.72 \pm 0.2) \times 10^{-2}$
1.10×10^8	$(1.13 \pm 0.2) \times 10^{-2}$	$(2.68 \pm 0.3) \times 10^{-2}$
1.20×10^8	$(1.69 \pm 0.2) \times 10^{-2}$	$(3.76 \pm 0.3) \times 10^{-2}$
1.32×10^8	$(1.83 \pm 0.2) \times 10^{-2}$	$(3.77 \pm 0.3) \times 10^{-2}$
1.45×10^8	$(1.98 \pm 0.3) \times 10^{-2}$	$(4.46 \pm 0.4) \times 10^{-2}$
1.59×10^8	$(2.32 \pm 0.3) \times 10^{-2}$	$(5.04 \pm 0.4) \times 10^{-2}$
1.74×10^8	$(2.73 \pm 0.3) \times 10^{-2}$	$(5.71 \pm 0.4) \times 10^{-2}$
1.91×10^8	$(3.21 \pm 0.3) \times 10^{-2}$	$(6.41 \pm 0.5) \times 10^{-2}$
2.09×10^8	$(3.62 \pm 0.4) \times 10^{-2}$	$(6.63 \pm 0.5) \times 10^{-2}$
2.29×10^8	$(4.00 \pm 0.4) \times 10^{-2}$	$(8.17 \pm 0.5) \times 10^{-2}$
2.51×10^8	$(4.94 \pm 0.4) \times 10^{-2}$	$(7.87 \pm 0.5) \times 10^{-2}$
2.76×10^8	$(4.79 \pm 0.4) \times 10^{-2}$	$(1.00 \pm 0.06) \times 10^{-1}$
3.02×10^8	$(6.16 \pm 0.5) \times 10^{-2}$	$(1.02 \pm 0.06) \times 10^{-1}$
3.31×10^8	$(6.16 \pm 0.5) \times 10^{-2}$	$(1.21 \pm 0.07) \times 10^{-1}$
3.63×10^8	$(7.58 \pm 0.6) \times 10^{-2}$	$(1.27 \pm 0.07) \times 10^{-1}$
3.99×10^8	$(7.64 \pm 0.6) \times 10^{-2}$	$(1.28 \pm 0.07) \times 10^{-1}$
4.37×10^8	$(9.16 \pm 0.7) \times 10^{-2}$	$(1.49 \pm 0.08) \times 10^{-1}$
4.79×10^8	$(9.15 \pm 0.7) \times 10^{-2}$	$(1.49 \pm 0.08) \times 10^{-1}$
5.25×10^8	$(9.70 \pm 0.7) \times 10^{-2}$	$(1.62 \pm 0.09) \times 10^{-1}$
5.76×10^8	$(1.05 \pm 0.08) \times 10^{-1}$	$(1.76 \pm 0.09) \times 10^{-1}$
6.32×10^8	$(1.08 \pm 0.08) \times 10^{-1}$	$(1.72 \pm 0.10) \times 10^{-1}$
6.93×10^8	$(1.16 \pm 0.08) \times 10^{-1}$	$(1.58 \pm 0.09) \times 10^{-1}$
7.59×10^8	$(1.21 \pm 0.09) \times 10^{-1}$	$(1.76 \pm 0.10) \times 10^{-1}$
8.33×10^8	$(1.08 \pm 0.09) \times 10^{-1}$	$(1.56 \pm 0.10) \times 10^{-1}$
9.13×10^8	$(1.10 \pm 0.09) \times 10^{-1}$	$(1.71 \pm 0.10) \times 10^{-1}$
1.00×10^9	$(1.16 \pm 0.10) \times 10^{-1}$	$(1.43 \pm 0.10) \times 10^{-1}$

C. The ^{209}Bi(n, f) cross section

The final (n, f) cross section for ^{209}Bi, extended for first time up to 1 GeV, is shown in Fig. 8. Earlier results obtained by Laptev *et al.* [19], Nolte *et al.* [26], Ryzhov *et al.* [27], Smirnov *et al.* [17], Fomichev *et al.* [29], and Gondalskiy *et al.* [28] with neutrons from threshold energy up to 200 MeV are also provided and are in agreement with our data. Data from Fomichev *et al.* are available up to 400 MeV and are compatible with our results within the statistical uncertainties. However, there is a discrepancy between our findings and those of Goldanskiy *et al.* at 380 MeV.

For energies above 200 MeV, previous experimental data for the (p, f) reaction [18] are higher than the present results at all energies. As expected, the Prokofiev systematics [21] for proton-induced fission shows agreement with our data at the highest energies.

VI. UPDATING FISSION CROSS SECTION SYSTEMATICS

A universal parametrization for neutron-induced fission in the subactinides was proposed by Smirnov *et al.* [17]:

$$\sigma_f(E_n) = P_1 \exp[-(P_2/E_n)^{P_3}], \quad (6)$$

where P_1, P_2, and P_3 are fitting parameters that depend on the target nuclei. This suggested set of parameters fits all the previous results and also our data below 200 MeV, but it underestimates the fission cross sections above that energy, as shown in Figs. 7 and 8.

As was mentioned before, the ^{209}Bi(n, f) cross section has been recommended as a standard by the International Atomic Energy Agency (IAEA) [2]. It was proposed as a substitution for the ENDF/HE-VI evaluation, which is based on the work of Fukahori and Pearlstein [30] and does not fit experimental results obtained since then. For the sake of simplicity in the graphs, we did not include this evaluation in the figure. The IAEA standard cross section based on the work of Carlson *et al.* [2] reproduces our results and the previous data below 200 MeV and even in the subthreshold region [28,31–34], but it underestimates the new data presented here and those of Fomichev *et al.* [29]. The original parametrization of Smirnov *et al.* [17] fits well up to 200 MeV, but above this energy it underestimates the cross section for both ^{nat}Pb and ^{209}Bi.

With the new set of parameters indicated in Table IV, we can use the same function [Eq. (6)] used by Smirnov *et al.* [17] to extend the parametrization of the ^{nat}Pb and ^{209}Bi fission cross sections up to 1 GeV while maintaining the agreement below 200 MeV (see Figs. 7 and 8).

The resulting parametrization for the $\sigma_f(^{nat}\text{Pb})/\sigma_f(^{209}\text{Bi})$ ratio is shown in Fig. 9. It agrees with the original parametrization of Smirnov *et al.* [17] between around 100 and 200 MeV, but it is higher above this energy. At around 1 GeV and above, our parametrization shows a tendency toward the Prokofiev systematics [21] for proton-induced fission, where the proton- and neutron-induced cross sections are expected to converge.

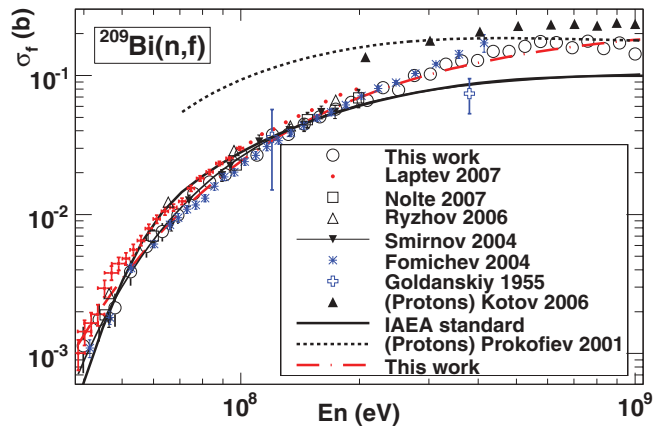

FIG. 8. (Color online) Neutron-induced fission cross section for ^{209}Bi obtained at the n_TOF facility. Earlier results using neutrons [17,19,26–29] are shown for comparison. The parametrization of Ref. [17] and our parametrization are also shown (see Sec. VI). Experimental results [18] and a parametrization [21] for protons are indicated as well. The thick solid line corresponds to the IAEA standard fission cross section [2].

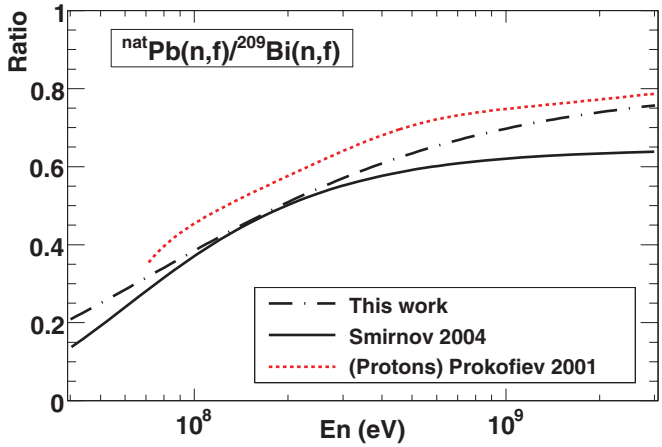

FIG. 9. (Color online) Fission cross section ratio $\sigma_f(^{\text{nat}}\text{Pb})/\sigma_f(^{209}\text{Bi})$ given by different parametrizations [17,21] compared to the new one proposed in this work.

VII. SUMMARY AND CONCLUSIONS

The $^{\text{nat}}\text{Pb}(n,f)$ and $^{209}\text{Bi}(n,f)$ cross sections were measured at the n_TOF facility from threshold energy up to 1 GeV, the highest energy reached to date. A fission chamber was developed for this purpose and the fission fragments were detected in coincidence using PPACs. The cross sections were measured relative to ^{235}U and ^{238}U and were converted into absolute values using the JENDL/HE-2007 evaluation. The results obtained from both reference cross sections ^{235}U and ^{238}U were compatible, so the average was used for the final values. The reliability of our method is also supported by results obtained for other nuclei in the same experiment, such as ^{234}U and ^{237}Np [3].

TABLE IV. Proposed parameters of the $^{\text{nat}}\text{Pb}(n,f)$ $^{209}\text{Bi}(n,f)$ cross sections for Eq. (6).

Nuclide	P_1	P_2	P_3	χ^2/ν
$^{\text{nat}}$Pb	198.9	379.2	0.839	0.65
^{209}Bi	250.0	259.0	0.895	1.46

Our data are in good agreement with previous experimental data up to 200 MeV. Above this energy and up to 1 GeV, where no data were previously available, our results exhibit important differences when compared to recent parametrizations, such as those of Smirnov *et al.* [17] and the IAEA standard based on the work of Carlson *et al.* [2], which were fitted to the data available below 200 MeV.

The results of this work are here proposed as a new parametrization for the $^{\text{nat}}\text{Pb}(n,f)$ and $^{209}\text{Bi}(n,f)$ cross sections covering the energy range up to 1 GeV, for the purpose of updating existing neutron fission cross section evaluations in the intermediate- and high-energy region.

ACKNOWLEDGMENTS

This work was partially supported by the EC under Contract No. FIKW-CT-2000-00107 and by the Spanish Ministerio de Educación under Grant No. FPU-AP2007-04542.

[1] Accelerator and Spallation Target Technologies for ADS Applications. A Status Report. OECD/NEA Report No. 5421, NEA, 2005.
[2] A. D. Carlson, S. Chiba, F. J. Hambsch, N. Olsson, and A. N. Smirnov, Update to nuclear data standards for nuclear measurements, INDC (NDS)-368, IAEA-NDS, Vienna, 1997, available at [http://www-nds.iaea.org/reports-new/indc-reports/indc-nds/indc-nds-0368.pdf].
[3] C. Paradela *et al.*, Phys. Rev. C **82**, 034601 (2010).
[4] L. Audouin *et al.* (the n_TOF Collaboration), in *Proceedings of the International Conference on Nuclear Data for Science and Technology, April 22-27, 2007* (EDP Sciences, Nice, France, 2008) pp. 421–424.
[5] n_TOF Collaboration, CERN/SPSC 99-8 SPSC/P310, 1999 (CERN, Geneva, 1999).
[6] U. Abbondanno *et al.*, Report No. CERN-SL-2002-053 ECT, 2002 (CERN, Geneva, 1999).
[7] C. Borcea *et al.*, Nucl. Instrum. Methods A **513**, 524 (2003).
[8] C. Stephan, L. Ferrant, B. Berthier, S. David, L. Tassan-Got, C. O. Bacri, F. Rejmund, and C. Moreau (n_TOF Collaboration), Nucl. Sci. Tech. Suppl. **2**, 276 (2002).
[9] L. Tassan-Got, B. Berthier, I. Duran, L. Ferrant, S. Isaev, C. de la Naour, C. Paradela, C. Stephan, and D. Trubert (n_TOF Collaboration), in *Proceedings of the Conference on the Nuclear Data for Science and Technology, Santa Fe* (AIP Conference Proceedings, 2004), Vol. 1, p. 1529.
[10] L. Tassan-Got *et al.* (unpublished).
[11] L. Ferrant, Ph.D. thesis, Université Paris XI Orsay, 2005.
[12] H. Noshad *et al.*, J. Nucl. Sci. Technol. **38**, 901 (2001).
[13] V. E. Viola, K. Kwiatkowski, and M. Walker, Phys. Rev. C **31**, 1550 (1985).
[14] V. P. Eismont, A. V. Prokofiev, I. V. Ryzhov, A. N. Smirnov, G. A. Tutin, H. Condé, K. Elmgren, and N. Olsson, in *Proceedings of the 3rd International Conference on Accelerator Driven Transmutation Technologies and Applications, Praha, Czech Republic* (1999).
[15] G. Tutin *et al.*, Nucl. Instrum. Methods A **457**, 646 (2001).
[16] EXFOR (Experimental Nuclear Reaction Data). National Nuclear Data Center, Brookhaven, (2009) [http://www-nds.iaea.org/exfor/exfor.html].
[17] A. N. Smirnov *et al.*, Phys. Rev. C **70**, 054603 (2004).
[18] A. A. Kotov *et al.*, Phys. Rev. C **74**, 034605 (2006).
[19] A. B. Laptev, O. A. Shcherbakov, A. S. Vorobyev, R. C. Haight, and A. D. Carlson in *Proceedings of the 4th International Conference on Fission and Properties of Neutron-Rich Nuclei, Sanibel Island, Florida, 2007* (World Scientific, USA, 2007).
[20] O. Shcherbakov *et al.*, J. Nucl. Sci. Technol. Suppl. **2**, 230 (2002).
[21] A. V. Prokofiev, Nucl. Instrum. Methods A **463**, 557 (2001).
[22] V. P. Eismont *et al.*, Phys. Rev. C **53**, 2911 (1996).
[23] A. V. Prokofiev, Ph.D. thesis, Uppsala University, 2001.
[24] A. D. Carlson *et al.*, Nucl. Data Sheets **110**, 3215 (2009).
[25] T. Fukahori *et al.*, J. Nucl. Sci. Technol. (to be published) [http://wwwndc.jaea.go.jp].

[26] R. Nolte, M. S. Allie, F. D. Brooks, A. Buffler, V. Dangendorf, J. P. Meulders, H. Schuhmacher, F. D. Smit, and M. Weierganz, Nucl. Sci. Eng. **156**, 197 (2007).
[27] I. V. Ryzhov *et al.*, Nucl. Instrum. Methods A **562**, 439 (2006).
[28] V. I. Goldanskiy, V. S. Penkina, and E. Z. Tamurov, Dokl. Akad. Nauk **101**, 1027 (1955).
[29] A. V. Fomichev, V. N. Dushin, S. M. Soloviev, A. A. Fomichev, and S. Mashnik, Leningrad Report No. 262, EXFOR Entry 41444004, 2004 (unpublished).
[30] T. Fukahori and S. Pearlstein, in *Proceedings of the Advisory Group Meeting Organized by the IAEA, INDC(NDS)-245*, edited by N. P. Kocherov (IAEA-NDS, Vienna, 1990), p. 93.
[31] P. E. Vorotnikov and L. S. Larionov, Yad. Fiz. **40**, 867 (1984).
[32] R. H. Iyer, R. Sampathkumar, and N. K. Chaudhuri, Prog. Rep. BARC Trombay Rep. Ser. **872**, 107 (1976).
[33] Bao Zon-Gyu and Li Ji-Zhou, Chin. J. Nucl. Phys. **3**, 249 (1981) [Chin. Phys. **2**, 778 (1982)].
[34] R. Ganapathy and J. L. Meason, Radiochim. Acta **4**, 113 (1965).